One-Dimensional Micromechanical Analysis of Woven Fabric Composites

Takashi Ishikawa* and Tsu-Wei Chou†
University of Delaware, Newark, Delaware

The upper and lower bounds of elastic stiffness and compliance constants of woven fabric composites are derived, based upon a mosaic-like model as well as the assumptions of constant stress and constant strain. An approximate analysis taking into account fiber undulation and continuity also is conducted. Fiber undulation leads to a slight softening of the in-plane stiffness and does not affect the stretching/bending coupling constants. A transverse shear deformation is adopted and modified to examine the one-dimensional bending response of fabric composites. The results of a two-dimensional finite element analysis are in good agreement with the predictions of the in-plane, coupling, and bending constants based upon the fiber undulation, mosaic, and transverse shear deformation theory, respectively. The effect of fiber undulation shape on the in-plane compliance also is investigated.

Nomenclature

$A_{ij}(x), \bar{A}_{ij}$	= local and averaged in-plane stiffness
$a^*_{ij}(x), \bar{a}^*_{ij}$	= local and averaged in-plane compliance
a	= width of a thread
a_u	= length of undulation
$B_{ij}(x), \bar{B}_{ij}$	= local and averaged bending/stretching coupling stiffness
$b^*_{ij}(x), \bar{b}^*_{ij}$	= local and averaged bending/stretching coupling compliance
$D_{ij}(x), \bar{D}_{ij}$	= local and averaged bending stiffness
$d^*_{ij}(x), \bar{d}^*_{ij}$	= local and averaged bending compliance
E	= Young's modulus
G	= shear modulus
h	= thickness of a fabric composite plate
$h_1(x)$	= shape function of undulation
k	= a parameter for the transverse shear deformation theory
N_i	= membrane stress resultant
M_i	= moment resultant
n_g	= number of geometrical repeats in fabric structure
P_0	= lateral pressure in cylindrical bending
Q_{ij}	= elastic stiffness matrix
u,v,w	= displacement in the x,y,z, directions, respectively
x,y,z	= Cartesian coordinates
ϵ^0_i	= strain components at the geometrical midplane
κ_i	= curvature at the geometrical midplane
$\theta(x)$	= local off-axis angle in fiber undulation
ν	= Poisson's ratio
Superscripts	
F	= quantities of a fill thread
w	= quantities of a warp thread
$\alpha\alpha$	= quantities of a cross-ply laminate consisting of α material

Received Oct. 19, 1981; revision received June 7, 1982.

*Research Associate, Mechanical and Engineering Deparment (on leave from National Aerospace Laboratory, Tokyo, Japan). Member AIAA.

†Professor, Mechanical and Aerospace Engineering Department.

I. Introduction

WOVEN fabrics constitute an important form of reinforcement for plastic matrix materials. Conventional orthogonal weave fabrics provide bidirectional reinforcement in a single layer, have better impact resistance than tape laminates, and provide more balanced properties in the fabric plan than unidirectional laminae.[1] Although the structural efficiency of fabrics is not as great as that of unidirectional fibers, the ease of application and the resulting low fabrication cost have made fabrics attractive for structural applications.

In spite of the ever-increasing use of woven fabric composites, there is a lack of fundamental understanding of their thermo-mechanical behavior. The purpose of this paper is to investigate the corrlation between fabric structure and elastic properties. To facilitate the discussion, a brief review of the geometrical aspect of woven fabrics is provided.

All fabrics are formed by interlacing two sets of threads. The pattern of interlacing can be understood from the two-dimensional representations of Fig. 1, where the vertical and horizontal threads are known as the warp and fill threads, respectively.[2,3] The various types of weaves can be identified by the repeating patterns in both directions, defined by the two geometrical quantities n^F_g and n^w_g. The number n^F_g indicates that a warp thread is interlaced with every n^F_g-th fill thread. Likewise, n^w_g means that a fill thread is interspersed with every n^w_g-th warp thread. From here on, only the term "interlaced" will be used to denote the area where the fill and warp threads cross over each other as shown in Fig. 1. The present analysis is restricted to the case of $n^w_g = n^F_g = n_g$. Because this study is restricted to fabrics with only one type of fiber, no material parameters such as thread width ratio and relative fiber volume fraction need be considered.[5] Fabrics with $n_g \geq 4$ and with interlaced regions that are not connected are known as satin weaves. As defined by their n_g values, the fabrics of Fig. 1 are known as plain weave ($n_g = 2$), twill weave ($n_g = 3$), four-harness satin ($n_g = 4$), and eight-harness satin ($n_g = 8$).

Ishikawa[4] and Ishikawa and Chou[5] first adopted a mosaic model to derive the upper and lower bounds of elastic moduli of nonhybrid as well as hybrid fabric composites. This approach is different from that of some existing theories by, for instance, Kimpara,[6] Hirai and Senba,[7] and Kabelka.[8] The basis of idealization of the mosaic model can be seen from Fig. 2. Figure 2a is a cross-sectional view of an eight-harness satin. The consolidation of the fabric with a resin matrix material is depicted in Fig. 2b, which can be simplified by the

mosaic model of Fig. 2c. The key idealization of the mosaic model is the omission of the fiber continuity and undulation that exists in an actual fabric. A brief description of this analysis approach is given in Sec. II. One of the objectives of this paper is to assess the validity and applicability of the mosaic model and the problems resulting from the simplifications. A one-dimensional model that takes into account the effects of fiber undulation and continuity is developed in the present analysis. However, for large n_g values, such as in the case of eight-harness satin weave composites, this one-dimensional analysis of a strip-like material is not suitable to obtain the two-dimensional elastic properties in general.

Another objective of this paper is to consider the transverse shear deformation that has a significant effect on the bending rigidity of fabric composite plates. The theory developed by Yang, Norris, and Stavsky[9] and extended by Whitney and Pagano[10] is adopted for the present analysis.

Finally, some finite element calculations are also carried out to confirm the validity of the fiber undulation model and approximation involved in the transverse shear calculations. Then, general conclusions are drawn regarding the predictions of elastic properties of woven fabric composites based upon these various approaches.

II. Mosaic Model and Bound Approach

As shown in Fig. 2c, the continuity of fibers in the thread direction is neglected in the mosaic model. A fabric composite idealized by the mosaic model (Fig. 3a) can thus be regarded as an assemblage of pieces of asymmetrical cross-ply laminates (Fig. 3b). Based upon classical laminated plate theory under the assumption of Kirchhoff-Love hypothesis, the constitutive equations are written[11-13] for $i, j = 1, 2, 6$ as

$$\begin{bmatrix} N_i \\ M_i \end{bmatrix} = \begin{bmatrix} A_{ij} & B_{ij} \\ B_{ij} & D_{ij} \end{bmatrix} \begin{bmatrix} \epsilon_j^0 \\ \kappa_j \end{bmatrix} \tag{1}$$

or, in the inverted form

$$\begin{bmatrix} \epsilon_i^0 \\ \kappa_i \end{bmatrix} = \begin{bmatrix} a_{ij}^* & b_{ij}^* \\ b_{ij}^* & d_{ij}^* \end{bmatrix} \begin{bmatrix} N_j \\ M_j \end{bmatrix} \tag{2}$$

In Fig. 1 the repeating region of each fabric is enclosed by dashed lines. Also, in Fig. 1 the top side of the fabric is dominated by the fill threads, whereas the bottom side is dominated by the warp threads. Figure 3a depicts the mosaic model of a repeating region of an eight-harness satin weave. In the bound approach, the two-dimensional extent of the plate is simplified by considering two one-dimensional models where the pieces of cross-ply laminates are either in parallel or in series as shown in Figs. 3c and 3d.

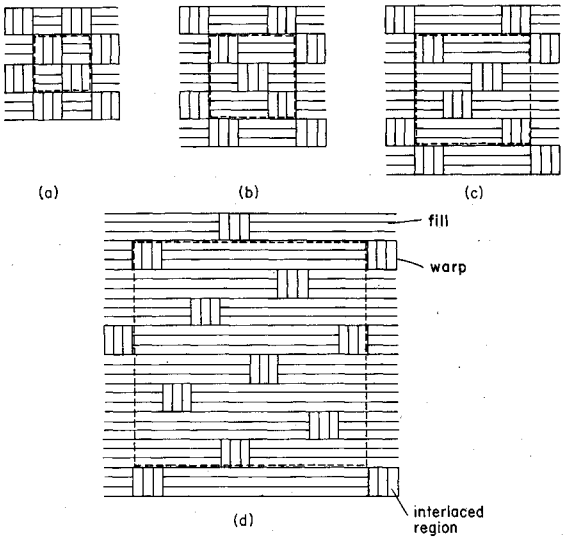

Fig. 1 Examples of woven fabrics: a) plain weave ($n_g = 2$), b) twill weave ($n_g = 3$), c) four harness satin ($n_g = 4$), and d) eight harness satin ($n_g = 8$).

In the parallel model, a constant strain state in the laminate midplane is assumed as a first approximation. For the one-dimensional repeating region of length $n_g a$, where a denotes the thread width, an average membrane stress $\bar{N}_1$ is defined as

$$\bar{N}_1 = \frac{1}{n_g a} \int_0^{n_g a} N_1 dy = A_{11}^{\alpha\alpha} \epsilon_1^0 + A_{12}^{\alpha\alpha} \epsilon_2^0 + \left(1 - \frac{2}{n_g}\right) B_{11}^{\alpha\alpha} \kappa_1 \tag{3}$$

where the factor $[1 - (2/n_g)]$ appears because the terms $B_{ij}^{\alpha\alpha}$ for the interlaced and noninterlaced regions have opposite signs. Other average stress and moment resultants can be derived in a similar manner. Let $\bar{A}$, $\bar{B}$, and $\bar{D}$ be the stiffness matrices relating the average stress resultants $\bar{N}$ and moment resultant $\bar{M}$, with ϵ^0 and κ. We obtain

$$\bar{A}_{ij} = A_{ij}^{\alpha\alpha}, \quad \bar{B}_{ij} = \left(1 - \frac{2}{n_g}\right) B_{ij}^{\alpha\alpha}, \quad \bar{D}_{ij} = D_{ij}^{\alpha\alpha} \tag{4}$$

These components provide upper bounds to the stiffness constants of the fabric composite based upon the one-dimensional model. If these stiffness constants are inverted, lower bounds of the elastic compliance constants can be obtained. All the elastic stiffness constants A, B, and D are computed based upon the basic laminate where the top layer is the fill threads (Fig. 3b).

In the series model, the disturbance of stress and strain near the interface of the interlaced region is neglected. Let the model be subjected to an in-plane force N_1 in the longitudinal direction. The assumption of constant stress leads to the definition of an average curvature

$$\bar{\kappa}_1 = \frac{1}{n_g a} \int_0^{n_g a} \kappa_1 dx = \left(1 - \frac{2}{n_g}\right) b_{11}^{*\alpha\alpha} N_1 \tag{5}$$

Let $\bar{a}^*$, $\bar{b}^*$, and $\bar{d}^*$ be the compliance matrices relating the average midplane strain ϵ^0 and curvature κ with the stress resultant $\bar{N}$ and moment resultant $\bar{M}$. Thus,

$$\bar{b}_{ij}^* = [1 - (2/n_g)] b_{ij}^{*\alpha\alpha}$$

$$\bar{a}_{ij}^* = a_{ij}^{*\alpha\alpha}, \qquad \bar{d}_{ij}^* = d_{ij}^{*\alpha\alpha} \tag{6}$$

Equations (6) give the upper bounds of the composite compliance constants and, after inversion, the lower bounds of the stiffness constants. In summary, both upper and lower bounds of the elastic stiffness and compliance constants can be obtained from the mosaic model.

III. Fiber Undulation Model

To consider the continuity and undulation of fibers in a fabric, a fiber undulation model (FUM) is developed in this

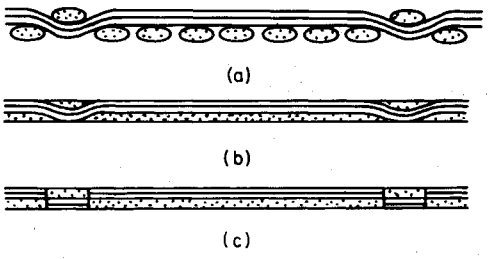

Fig. 2 Idealization of the mosaic model: a) cross-sectional view of a woven fabric before resin impregnation, b) woven fabric composite, and c) the idealization of the mosaic model.

section. Figure 4 depicts the geometry of fiber undulation expressed in the form of $h_1(x)$ with the length of a_u. The thickness of the undulated fill thread is $h/2$, one-half of the plate thickness h. The value of a_u can be arbitrary in the range from 0 to a. If a_u is specified, the locations of the points a_0 and a_2 are automatically determined by the relations $a_0=(a-a_u)/2$ and $a_2=(a+a_u)/2$.

The theoretical analysis is again performed based upon classical laminated plate theory. The model is essentially an extension of the series model used for the derivation of the upper bound of the compliance constants (Fig. 3d). However, unlike the previous case, a_{ij}^*, b_{ij}^*, and d_{ij}^* depend on the coordinate x. For a uniformly applied in-plane stress resultant N_1, the average in-plane compliance of the composite is defined by

$$\bar{a}_{ij}^*=\frac{2}{n_g a}\int_0^{n_g a/2} a_{ij}^*(x)\,dx \tag{7}$$

Because $a_{ij}^*(x)$ is a constant within the straight portion of Fig. 4, Eq. (7) can be modified as

$$\bar{a}_{ij}^*=\left(1-\frac{2a_u}{n_g a}\right)a_{ij}^{*\alpha\alpha}+\frac{2}{n_g a}\int_{a_0}^{a_2} a_{ij}^*(x)\,dx \tag{8}$$

Note that $a_{ij}^{*\alpha\alpha}$ denotes the in-plane compliance for the straight portion. The other compliance coefficients, $\bar{b}_{ij}^*$ and $\bar{d}_{ij}^*$ can be obtained in a similar manner,

$$\bar{b}_{ij}^*=\left\{\left[\left(\frac{n_g-1}{2}a-\frac{a_u}{2}\right)-\left(\frac{a}{2}-\frac{a_u}{2}\right)\right]b_{ij}^{*\alpha\alpha}+\int_{a_0}^{a_2} b_{ij}^*(x)\,dx\right\}\Big/\left(\frac{n_g a}{2}\right)=\left(1-\frac{2}{n_g}\right)b_{ij}^{*\alpha\alpha}+\frac{2}{n_g a}\int_{a_0}^{a_2} b_{ij}^*(x)\,dx \tag{9}$$

$$\bar{d}_{ij}^*=\left(1-\frac{2a_u}{n_g a}\right)d_{ij}^{*\alpha\alpha}+\frac{2}{n_g a}\int_{a_0}^{a_2} d_{ij}^*(x)\,dx \tag{10}$$

Equations (8-10) coincide with the upper bounds of the compliance in Eqs. (6) as a_u tends to zero. Thus, the problem is now reduced to the evaluations of the integrations in Eqs. (8-10).

The angle between the local fiber orientation and the global coordinate system, denoted by $\theta(x)$, is

$$\theta(x)=\arctan[dh_1(x)/dx] \tag{11}$$

The nonvanishing of this angle implies a reduction of the effective elastic constant in the x direction of the fill thread. Two methods are used for the evaluation of such reduction. The first method is to use the following two-dimensional transformation formulas of off-axis elastic moduli[14]

$$\begin{aligned}
F_x^F(\theta)&=1/\{\ell_\theta^4/E_x^F+(1/G_{xz}^F-2\nu_{zx}^F/E_x)\ell_\theta^2 m_\theta^2+m_\theta^4/E_z^F\}\\
\nu_{yx}^F(\theta)&=\nu_{zx}^F\ell_\theta^2+\nu_{yz}^F m_\theta^2\\
G_{xy}^F(\theta)&=G_{xy}^F\ell_\theta^2+G_{yz}^F m_\theta^2\\
E_y^F(\theta)&=E_y^F=E_z^F
\end{aligned} \tag{12}$$

where $\ell_\theta=\cos\theta$, $m_\theta=\sin\theta$. Note that the transverse isotropy in the y-z plane of the fill thread is taken into account. The local stiffness of the undulated portion is thus given by

$$Q_{ij}^F(\theta)=\begin{bmatrix} E_x^F(\theta)/D_\nu & E_y^F\nu_{yx}^F(\theta)/D_\nu & 0\\ E_y^F\nu_{yx}^F(\theta)/D_\nu & E_y^F/D_\nu & 0\\ 0 & 0 & G_{xy}^F(\theta)\end{bmatrix} \tag{13}$$

where $i,j=1,2,6$ and $D_\nu=1-\nu_{yx}^F(\theta)^2 E_y^F/E_x^F(\theta)$.

The second method is to directly transform Q_{ij}^F of the nonundulated thread as,

$$\begin{aligned}
Q_{11}^F(\theta)&=Q_{11}^F\ell_\theta^4+2Q_{13}^F\ell_\theta^2 m_\theta^2+Q_{33}^F m_\theta^4+4Q_{55}^F\ell_\theta^2 m_\theta^2\\
Q_{66}^F(\theta)&=Q_{66}^F\ell_\theta^2+Q_{44}^F m_\theta^2\\
Q_{12}^F(\theta)&=Q_{12}^F\ell_\theta^2+Q_{23}^F m_\theta^2\\
Q_{22}^F(\theta)&=Q_{22}^F\quad\text{other}\quad Q_{ij}=0
\end{aligned} \tag{14}$$

Comparisons of the approaches as represented in Eqs. (13) and (14) are given in Sec. VI.

Once these transformation formulas are established, the local plate moduli, $A_{ij}(x)$, $B_{ij}(x)$, and $D_{ij}(x)$ can be easily calculated from

$$[A_{ij}(x),B_{ij}(x),D_{ij}(x)]=\int_{-h/2}^{h/2} Q_{ij}(\theta)\,(1,z,z^2)\,dz \tag{15}$$

namely,

$$\begin{aligned}
A_{ij}(x)&=\int_{-h/2}^{h_1(x)-h/2} Q_{ij}^W dz+\int_{h_1(x)-h/2}^{h_1(x)} Q_{ij}^F(\theta)\,dz\\
&\quad+\int_{h_1(x)}^{h/2} Q_{ij}^W dz=[Q_{ij}^W+Q_{ij}^F(\theta)]\cdot h/2\\
B_{ij}(x)&=\frac{h}{2}\left[\frac{h^2}{4}-hh_1(x)\right][Q_{ij}^W-Q_{ij}^F(\theta)]\\
D_{ij}(x)&=\frac{1}{3}Q_{ij}^W\left\{\frac{h^3}{8}-\frac{3}{2}h[h_1(x)]^2+\frac{3}{4}h^2h_1(x)\right\}\\
&\quad+\frac{1}{3}Q_{ij}^F(\theta)\left\{\frac{h^3}{8}+\frac{3}{2}h[h_1(x)]^2-\frac{3}{4}h^2h_1(x)\right\}
\end{aligned} \tag{16}$$

The local compliance coefficients, $a_{ij}^*(x)$, $b_{ij}^*(x)$, and $d_{ij}^*(x)$ can be obtained by inverting $A_{ij}(x)$, $B_{ij}(x)$, and $D_{ij}(x)$ in Eq. (16). Thus, we have explicit expressions of the integrands in Eqs. (8-10), although they are very lengthy. Therefore, these integrations will be evaluated by a numerical technique.

A shape of the undulation, $h_1(x)$, should be specified to simulate the actual configuration. The following sinusoidal function

$$h_1(x)=\left\{\sin\left[\left(x-\frac{a}{2}\right)\frac{\pi}{a_u}\right]+1\right\}h/4 \tag{17}$$

is chosen for the purpose of illustration. The mosaic model can be described by a step function as

$$h_1(x)=\begin{cases}0; & x\le a/2\\ h/2; & a/2<x\end{cases} \tag{18}$$

Equation (18) is useful for checking the numerical calculations.

Because the present analysis considers a one-dimensional strip of a fabric, it is not suitable to determine nonaxial constants such as $\bar{a}_{12}^*$ as compared to axial constants. Reliable shear related constants such as $\bar{a}_{66}^*$ or $\bar{A}_{66}$ are obtained; however, they are not present in this paper for reasons of brevity.

IV. Transverse Shear Deformation

The aforementioned approximate theory based upon fiber undulation cannot satisfactorily predict the bending behavior as will be shown later, although it gives reasonable results for a_{ij}^* and b_{ij}^*. The main reason for this deficiency in d_{ij}^* is attributed to a transverse shear deformation, which is investigated in this section.

A survey of the literature concerning transverse shear can be found in Ref. 11. The theory developed by Yang, Norris, and Stavsky[9] and extended by Whitney and Pagano[10] is employed here because it is more suitable for the present approximation purposes than, for instance, the theory described by Ambartsumyan.[15]

A fundamental point of the theory of Ref. 10 is the introduction of ψ_x and ψ_y and the following assumption for the displacement field:

$$u=u^0(x,y)+z\psi_x(x,y)$$

$$v=v^0(x,y)+z\psi_y(x,y)$$

$$w=w(x,y) \tag{19}$$

where the superscript *0* denotes the quantities at a reference plane. Instead of $-\partial w/\partial x$ and $-\partial w/\partial y$ in the classical plate theory (CPT),[11,12] ψ_x and ψ_y are adopted in this theory, which is referred to as a modified shear deformation theory (MSDT). General governing equations are given in Refs. 9 and 10. If a cylindrical bending state is considered, the governing equations for the one-dimensional case can be simplified as follows:

$$A_{11}\frac{\partial^2 u^0}{\partial x^2}+B_{11}\frac{\partial^2\psi_x}{\partial x^2}=0$$

$$kA_{55}\left(\frac{\partial\psi_x}{\partial x}+\frac{\partial^2 w}{\partial x^2}\right)+p=0$$

$$B_{11}\frac{\partial^2 u^0}{\partial x^2}+D_{11}\frac{\partial^2\psi_x}{\partial x^2}-kA_{55}\left(\psi_x+\frac{\partial w}{\partial x}\right)=0 \tag{20}$$

where a parameter k is a factor for the transverse shear resultants.[10,16] The range of k from ⅔ to unity is recommended in Ref. 10. The value of ⅔ is employed in the present paper. The maximum deflection for a simply supported plate of a width $n_g a$ under applied load $p=p_0\sin\pi x/(n_g a)$, for example, is

$$w_{\max}=w'_{\max}+p_0 n_g^2 a^2/\pi^2 kA_{55} \tag{21}$$

where $w'_{\max}$ is the CPT solution

$$w'_{\max}=A_{11}n_g^4 a^4 p_0/\pi^4(A_{11}D_{11}-B_{11}^2)$$

The in-plane extension under this load at $x=0$ is

$$u^0_{(x=0)}=B_{11}n_g^3 a^3 p_0/\pi^3(A_{11}D_{11}-B_{11}^2) \tag{22}$$

This theory, however, is not adequate for treating pure bending/extensional coupling problems without the applied load p. In fact, this modified shear deformation theory provides the identical solution to CPT under prescribed N_0 and M_0. In order to avoid this deficiency, the following modification to the theory of Ref. 10 is employed. We suppose that an increased bending deflection in Eqs. (21) and (22) can be attributed hypothetically to the modified plate moduli, A'_{11}, B'_{11}, and D'_{11}. It is also assumed that the modified moduli give the same in-plane extension. Thus, we have

$$\frac{A_{11}n_g^4 a^4}{\pi^4(A_{11}D_{11}-B_{11}^2)}+\frac{n_g^2 a^2}{\pi^2 kA_{55}}=\frac{A'_{11}n_g^4 a^4}{\pi^4(A'_{11}D'_{11}-B'^2_{11})}$$

$$\frac{B_{11}n_g^3 a^3}{\pi^3(A_{11}D_{11}-B_{11}^2)}=\frac{B'_{11}n_g^3 a^3}{\pi^3(A'_{11}D'_{11}-B'^2_{11})} \tag{23}$$

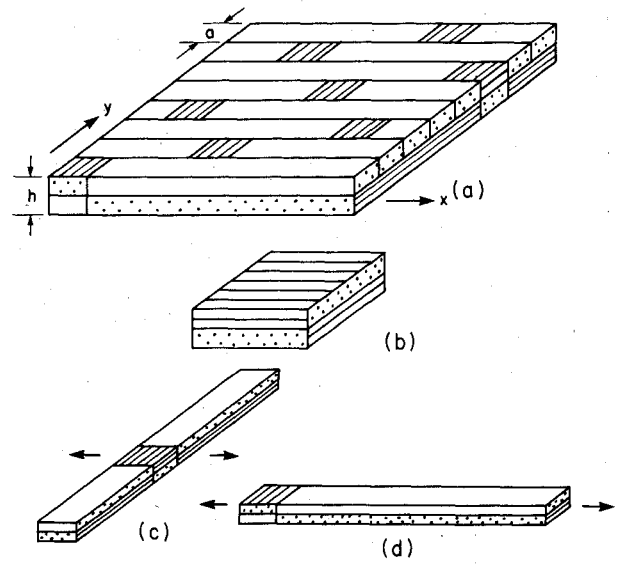

Fig. 3 Mosaic model of: a) repeating region in an eighth harness satin composite, b) a basic cross-ply laminate, c) parallel model, d) series model.

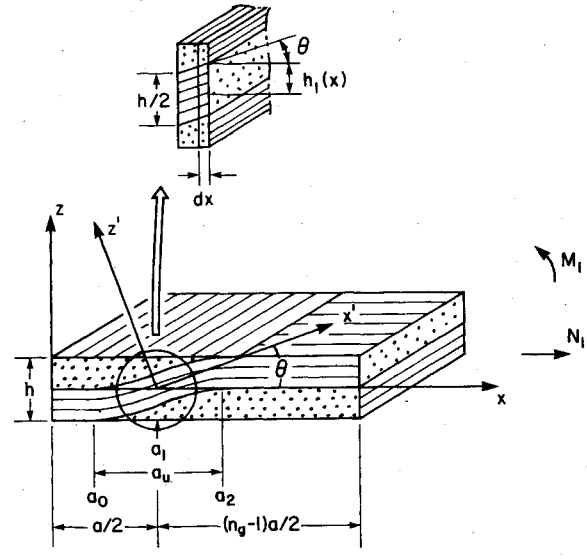

Fig. 4 Fiber undulation model.

Because B_{11} is not susceptible to the transverse shear effect as shown later, it can be assumed that $B_{11}=B'_{11}$. Thus,

$$A'_{11}=A_{11}+\frac{\pi^2(A_{11}D_{11}-B_{11}^2)}{n_g^2 a^2 kA_{55}}$$

$$D'_{11}=A_{11}D_{11}\Big/\left[A_{11}+\frac{\pi^2(A_{11}D_{11}-B_{11}^2)}{n_g^2 a^2 kA_{55}}\right] \tag{24}$$

Equation (24) represents a decrease in D'_{11} as well as an increase in A'_{11} due to the finite value of A_{55}. Equation (24) will be applied for a modification of the previous solution based on the mosaic model.

V. Finite Element Analysis

The applicability of the approximate theories presented in Secs. II-IV is examined by conducting a finite element analysis of the fiber undulation problem. The finite element computer program named EPIC-IV and developed by Yamada and Yokouchi[17] is modified for the present purpose. This program is suitable for static elastic-plastic analysis of plane stress,

plane strain, generalized plane strain, and axisymmetric problems. The capability of treating a generalized orthotropic material behavior is incorporated into the program. The transformation of elastic constants from the local coordinate system to the global system is required for finite element analysis of the fiber undulation problem.

Figure 5 depicts the geometry of two one-dimensional models used in the finite element analysis. The cases of $n_g = 2$, 3, and 4 are considered for the sake of economy in computing. The finite extent of the representative regions chosen for computation can reflect the one-dimensional behavior of the fabric composite when the boundary conditions are appropriately specified. At the left ends of the models in Fig. 5 the x displacement as well as the z displacement at the center node are prohibited. The boundary conditions at the right ends of the models are approximately satisfied by attaching to the boundary a tip region of an imaginary material with extremely high shear modulus of G_{xz}. The purpose of adding these tip regions is to insure that the end surfaces will remain straight under loading. Two types of loading on the tip region, uniform and pure bending (a linearly distributed load that vanishes at the midplane), are applied. Other boundary conditions, including ends without the tip regions, and concentrated instead of distributed loads are also examined. Preliminary results show that, as far as the left halves of the computation models are concerned, there is virtually no difference in the deformation and stress states with these different boundary conditions.

Figure 6a depicts a mesh subdivision for the fiber undulation model. The sinusoidal function of Eq. (17) is assumed for comparison purpose. Mesh patterns are shown in Fig. 6b, and they are adopted for the mosaic model according to the required accuracy. The convergence characteristics of these mesh patterns are discussed in Sec. VI. Also both plane stress and generalized plane strain conditions are considered to ascertain the Poisson's effect.

Material properties of a graphite-epoxy fabric composite at 60% of fiber volume fraction are given in Table 1 for numerical calculations. Note that the transverse isotropy in the y-z plane of the fill thread and in the x-z plane of the warp thread[7] is taken into account for properties required for the generalized plane strain state. Furthermore, the value of G_{xz} of the imaginary material is assumed to be nearly 10 times that of the fill thread for reasons mentioned before.

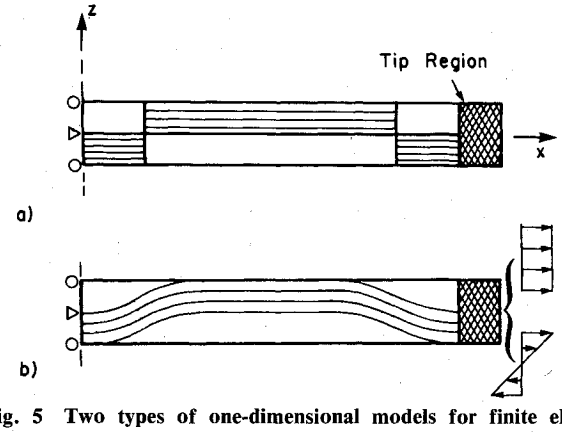

Fig. 5 Two types of one-dimensional models for finite element analysis: a) mosaic model and b) fiber undulation model.

Table 1 Properties of unidirectional graphite-epoxy material, GPa for moduli

Property	Warp	Fill	Tip region
E_x	8.82	113.00	196.00
E_z	8.82	8.82	8.82
ν_{zx}	0.495	0.3	0.4
G_{xz}	2.95	4.46	392.00
E_y	113.00	8.82	8.82
ν_{xy}	0.3	0.0235	0.018
ν_{yz}	0.0235	0.495	0.4
G_{xy}	4.46	4.46	392.00
G_{yz}	4.46	2.95	3.15

VI. Numerical Results

Numerical calculations are conducted for the case of graphite fabric in an epoxy matrix (Table 1). The geometrical parameters a, h, and a_u are chosen to be 1.0, 0.4, and 0.6 mm, respectively, unless otherwise stated. Although a comparison between theory and experiment is omitted here for the sake of brevity, Ref. 18 provides good correlation between analyses and experiments.

Convergence Characteristics of Finite Element Analysis

Convergence characteristics of the finite element analysis for the mosaic model of $n_g = 3$ are shown in Fig. 7. The a^*_{11} and b^*_{11} values are shown as functions of the number of nodes in the finite element mesh (N_{node}). N_{node} values corresponding to the mesh patterns of Fig. 6b are also indicated. The finite element results are compared in Fig. 7 with those of the upper bound predictions based upon the mosaic model [Eq. (6)]. The convergence is satisfactory for medium mesh size, and the overall agreement between these two approaches is reasonable considering the uniform stress resultant assumption in the derivation of the upper bounds of compliances and the requirement of the equilibrium of force in the x direction in the finite element analysis.

Results indicated by solid circles in Fig. 7 are based upon the plane stress assumption, whereas + denotes those for the generalized plane strain. There is almost no discrepancy between these two states. Therefore, from here on only plane stress results are presented, unless otherwise stated.

$\bar{a}^*_{11}$

Figure 8 shows the relationship between the in-plane compliance $\bar{a}^*_{11}$ and the inverse of the geometric repeat number n_g. Results of several different approaches are presented. The mosaic model (MM)[1] is used to predict the upper and lower bounds (UB and LB). The fiber undulation model (FUM) is applied to derive the reduced modulus (RM) from Eq. (13) and the reduced stiffness (RS) from Eq. (14). The finite element method (FEM) is applied to the two-dimensional mosaic model and fiber undulation model as well as the three-dimensional mosaic model.[4]

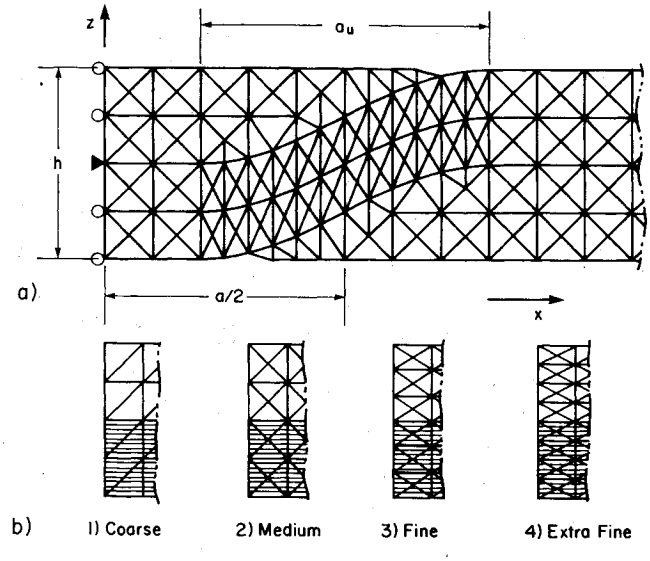

Fig. 6 Fiber undulation model: a) mesh subdivision ($a_u/h = 1.5$), b) mesh patterns.

The results of two-dimensional FEM-MM for $n_g = 2$, 3, and 4 agree well with those from the UB also derived from the MM. The approximate analysis of FUM-RM gives solutions much closer to those from the two-dimensional FEM-FUM than the FUM-RM analysis. The two-dimensional analysis also indicates that fiber undulation results in lower in-plane stiffness or higher $\bar{a}^*_{11}$ values, and that this finding is consistent with the predictions of the approximate methods of FUM-RM.

In Fig. 8, a three-dimensional finite element analysis (3-D FEM-MM) is also presented for an eight-harness satin weave composite. The result deviates significantly from that of the UB-MM. This fact implies that the present model is not fully descriptive of the mechanics in satin weave composites where n_g is large. Therefore, an improved analytical model is presented in Ref. 18 particularly for satin weave composites.

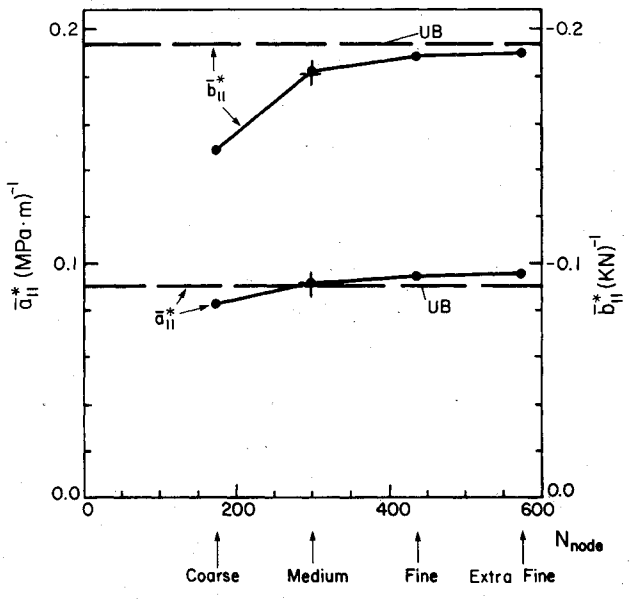

Fig. 7 Convergence characteristics of the finite element analysis for the mosaic model of $n_g = 3$ as functions of the number of nodes in the finite element mesh (N_{node}). †: Results of generalized plane strain state (see Sec. V).

Two opposing factors can affect the in-plane compliance. First, the elastic stiffness is reduced as can be seen from the results of Eq. (12) or (14). This reduction in stiffness gives rise to increase in the in-plane compliance. Second, the reduction of the local coupling effect due to fiber undulation leads to the decrease of in-plane compliance. It can be seen from Fig. 6, for instance, that the local coupling effect reduces from its maximum value at the nonundulated portion of the fill thread to zero at the midpoint of the undulated portion, where the arrangement of the fill and warp threads is symmetrical.

$\bar{b}^*_{11}$

The relationship between the coupling compliance $\bar{b}^*_{11}$ and $1/n_g$ is demonstrated in Fig. 9. The results from the approximate analyses of RM and RS coincide exactly with those of the UB prediction. This fact can be easily understood by considering the fact that the second term of Eq. (9) vanishes due to the assumed asymmetrical shape of fiber undulation and, hence, the odd-function representation of $b^*_{ij}(x)$ with respect to $x = a/2$.

The two-dimensional FEM analyses based upon the MM and FUM provide essentially identical results for $n_g = 2$, 3, and 4. Moreover, the two-dimensional FEM results are in good agreement with the UB predictions. Thus it can be concluded that symmetric fiber undulation such as the one assumed in Eq. (17) does not affect $\bar{b}^*_{11}$ and that the upper bound prediction based upon the mosaic model is adequate.

$\bar{d}^*_{11}$

Numerical results of $\bar{d}^*_{11}$ are given in Fig. 10. FEM solutions for both MM and FUM are extremely close to each other for the n_g values examined. Unlike in the cases of $\bar{a}^*_{11}$ and $\bar{b}^*_{11}$, the FEM solution results are quite different from those the UB approach, which is based upon classical plate theory (CPT). This is the reason why the modified shear deformation theory (MSDT) is introduced (Sec. IV). The results of this theory for the MM indicated by a dashed curve coincide fairly well with the FEM results, and the MSDT appears to be adequate for predicting $\bar{d}^*_{11}$.

Effect of Undulation Shape

Figure 11 demonstrates the effect of fiber undulation shape on $\bar{a}^*_{11}$ obtained by the approximate analyses of FUM-RM.

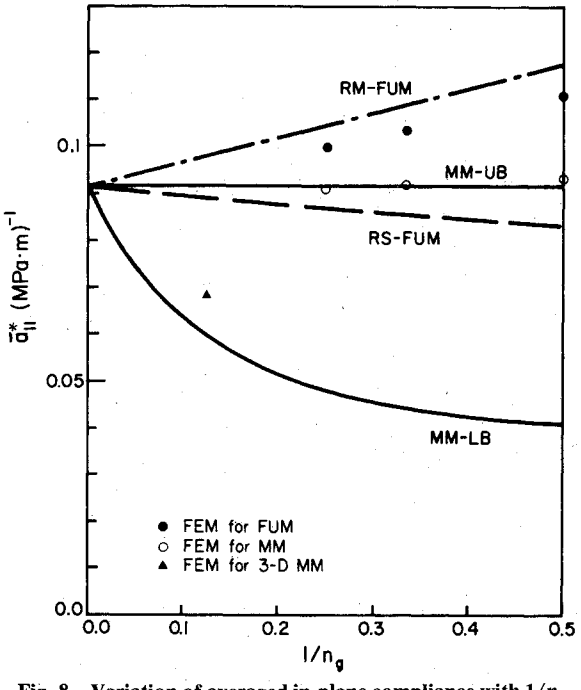

Fig. 8 Variation of averaged in-plane compliance with $1/n_g$.

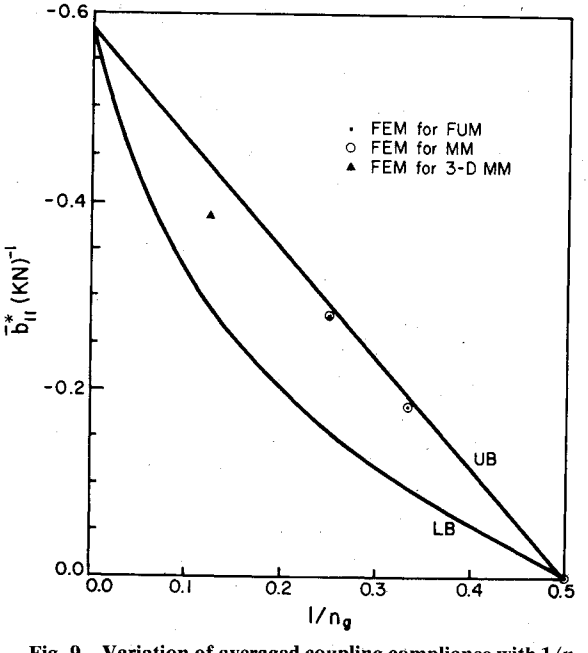

Fig. 9 Variation of averaged coupling compliance with $1/n_g$.

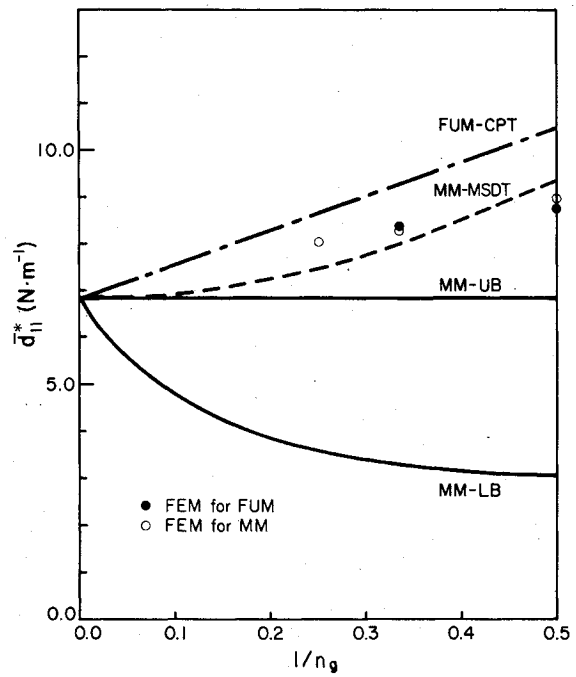

Fig. 10 Variation of averaged bending compliance with $1/n_g$.

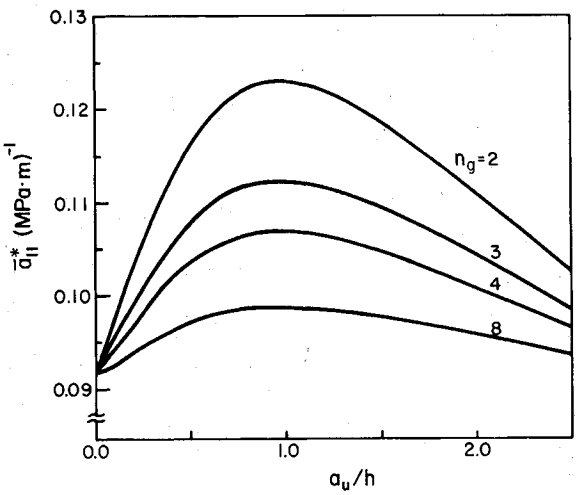

Fig. 11 Relationships between averaged in-plane compliance and undulation length.

The geometrical parameters a, a_u, and h are defined in Fig. 6. The calculations are performed for the range of a_u/h values from 0 to a/h, where the case $a_u=0$ corresponds to the configurations of a mosaic model. The results show that $\bar{a}_{11}^*$ is susceptible to the undulation shape, particularly at small n_g values. The highest $\bar{a}_{11}^*$ value, i.e., the lowest in-plane stiffness, is obtained at around $a_u/h=1$. On the other hand, the $\bar{a}_{11}^*$ values at $a_u/h=0$ and a/h are not far apart. Because in actual fabrics a_u may be fairly close to a and hence $a_u/h=a/h$, the mosaic model ($a_u/h=0$) seems to be a convenient model to evaluate the in-plane stiffness of a fabric.

VII. Conclusions

1) A fabric composite can be idealized as an assemblage of pieces of asymmetric cross-ply laminates. The upper and lower bounds of elastic stiffness and compliance of fabric composite plates in such a mosaic-like model are obtained based upon the constant strain and constant stress assumptions.

2) An approximate analysis which considers the undulation of fibers is conducted based upon a serial link model and classical plate theory. The results of $\bar{a}_{11}^*$ from the reduced modulus analysis demonstrate that fiber undulation leads to a slight softening in the in-plane stiffness as compared to the mosaic model. However, fiber undulation has no effect on the coupling constants. Therefore, the solutions of the coupling compliances based on the mosaic model can be considered to be reliable. The one-dimensional model developed in this paper is successful in assessing the effect of fiber undulation and continuity on the elastic properties of woven fabric composites. Both the results of the fiber undulation model and the mosaic model compare very favorably with the results of the finite element analyses conducted in the present work.

3) In the case of $\bar{D}_{11}^*$, a transverse shear deformation theory is adapted to examine the response of a fabric composite plate under both cylindrical bending and lateral force. For the purpose of the present problem, a modification to the plate moduli A_{11} and D_{11} is introduced. The results agree reasonably well with those obtained by the finite element analysis.

4) Several two-dimensional finite element analyses are carried out for a one-dimensional section of a fabric in order to confirm the aforementioned approximate theories. Convergence characteristics of the finite element analysis also are examined.

5) The effect of the shape of fiber undulation on the in-plane compliance is investigated. The results demonstrate that the values of $\bar{a}_{11}^*$ become close to those for the mosaic model when the undulation is extensive.

6) The bound theory based upon the mosaic model is useful for a rough estimation of fabric composite stiffness properties. The fiber undulation model provides a better prediction capabilities than the mosaic model covering in-plane and bending moduli. However, the fiber undulation model is inadequate for evaluation of the elastic behavior of satin weave composites with large n_g. For these a more refined analytical technique needs to be developed.[18]

Acknowledgment

This work is supported by the U.S. Army Research Office. The authors also wish to thank Dr. Y. Yokouchi for permission to use the EPIC-IV computer program and for his helpful discussions.

References

[1]Zweben, C., "Advanced Composites: A Revolution for the Designer," AIAA Paper, May 1981.

[2]Miller, E., *Textiles Properties and Behavior*, rev. ed., B. T. Batsford, London, 1976.

[3]Strong, J. M., *Foundations of Fabric Structures*, National Trade, 1953.

[4]Ishikawa, T., "Anti-Symmetric Elastic Properties of Composite Plates of Satin Weave Cloth," *Fibre Science and Technology*, Vol. 15, Sept. 1981, pp. 127-145.

[5]Ishikawa, T. and Chou, T. W., "Elastic Behavior of Woven Hybrid Composites," *Journal of Composite Materials*, Vol. 16, Jan. 1982, pp. 2-19.

[6]Kimpara, I., Hamamoto, A., and Takehana, M., "Analysis of First Knee Behavior of Woven Roving Composites," *Transactions of Japan Society of Composite Materials*, Vol. 3, Dec. 1977, pp. 21-26.

[7]Hirai, T. and Senba, T., "On the Mechanical Behavior of Fabric-Strengthened Composites Considering Three-Dimensional Cross-Linked Structure," *Advanced in Composite Materials, Proceedings of the Third International Conference on Composite Materials*, edited by A. R. Bunsell et al., Pergamon Press, New York, 1980, pp. 357-371.

[8]Kavelka, J., "Thermal Expansion of Composites with Canvas-Type Reinforcement and Polymer Matrix," *Advances in Composite Materials, Proceedings of the Third International Conference on Composite Materials*, edited by A. R. Bunsell et al., Pergamon Press, New York, 1980, pp. 770-782.

[9]Yang, P. C., Norris, C. H., and Stavsky, Y., "Elastic Wave Propagation in Heterogeneous Plates," *International Journal of Solids and Structures*, Vol. 2, Oct. 1966, pp. 665-684.

[10] Whitney, J. M. and Pagano, N. J., "Shear Deformation in Heterogeneous Anisotropic Plates," *Journal of Applied Mechanics*, Vol. 37, Dec. 1970, pp. 1031-1036.

[11] Jones, R. M., *Mechanics of Composite Materials*, McGraw-Hill Book Co., New York, 1975.

[12] Whitney, J. M. and Leissa, A. W., "Analysis of Heterogeneous Anisotropic Plates," *Journal of Applied Mechanics*, Vol. 36, June 1969, pp. 261-266.

[13] Tsai, S. W., "Structural Behavior of Composite Materials," NASA CR-71, July 1964.

[14] Lekhnitskii, S. G., *Theory of Elasticity of an Anisotropic Elastic Body*, Holden-Day, San Francisco, 1963.

[15] Ambartsumyan, S. A., *Theory of Anisotropic Plates*, edited by J. E. Ashton, translated by T. Cheron, Technomic, Stamford, Conn., 1970.

[16] Mindlin, R. D., "Influence of Rotatory Inertia and Shear on Flexural Motions of Isotropic Elastic Plates," *Journal of Applied Mechanics*, Vol. 18, March 1951, pp. 31-38.

[17] Yamada, Y. and Yokouchi, Y., *Finite Element Programming for Elastic-Plastic Analysis*, Baifu-Kan, Tokyo, 1981 (in Japanese).

[18] Ishikawa, T. and Chou, T. W., "Stiffness and Strength Behavior of Woven Fabric Composites," *Journal of Material Science*, in press.